Skeleton-Based Morphological Coding of Binary Images

Renato Kresch and David Malah

Department of Electrical Engineering
Technion-Israel Institute of Technology
Haifa 32000, Israel.

Proposed Running Title:

Skeleton-Based Coding of Binary Images

Key words:
Image coding
Binary images
Skeleton
Mathematical morphology

List of Symbols:
$\oplus$ - Binary dilation.
$\ominus$ - Binary erosion.
$\circ$ - Binary opening.
$\bullet$ - Binary closing.
$\mathcal{N}$ - The set of Natural numbers.
$\mathcal{Z}$ - The set of Integer numbers.
$\mathcal{R}$ - The set of Real numbers.
$\mathcal{F}$ - Family of shapes.
$\subseteq$ - Contained or equal to.
$\subset$ - Contained.
$\cup$ - Union.
$\cap$ - Intersection.

Number of pages in the article: 30
Number of Tables in the article: 2
Number of Figures in the article: 14

Skeleton-Based Morphological Coding of Binary Images*

Renato Kresch‡ and David Malah

Department of Electrical Engineering
Technion - Israel Institute of Technology
Haifa 32000, Israel.

ABSTRACT

This paper presents new properties of the discrete morphological skeleton representation of binary images, along with a novel coding scheme for lossless binary image compression that is based on these properties.

Following a short review of the theoretical background, two sets of new properties of the *discrete* morphological skeleton representation of binary images are proved. The first one leads to the conclusion that only the radii of skeleton points belonging to a subset of the ultimate erosions are needed for perfect reconstruction. This corresponds to a *lossless sampling* of the quench function. The second set of new properties is related to *deterministic prediction* of skeletonal information in a progressive transmission scheme.

Based on the new properties, a novel coding scheme for binary images is presented. The proposed scheme is suitable for progressive transmission and fast implementation. Computer simulations, also presented, show that the proposed coding scheme substantially improves the results obtained by previous skeleton-based coders, and performs better than classical coders, including run-length/Huffman, quadtree and chain coders. For facsimile images, its performance can be placed between the MR method ($K = 4$) and MMR method.

*This work was supported by the Fund for Promotion of Research at the Technion.

‡Presently at Hewlett-Packard Laboratories Israel, Technion, Haifa 32000, Israel. E-mail: renato@hp.technion.ac.il

1 Introduction

Mathematical morphology [27, 28, 7, 5, 24] is a relatively new, rapidly growing, nonlinear theory for image processing, based on set theory, and with a strong *geometric* orientation. It was developed by Matheron and Serra in the mid 1960s for describing the structure of materials by image analysis of their cross sections. Originally developed for binary images, it was later (during the 1970s) generalized for grayscale images as well [32]. For binary images, mathematical morphology provides a well-founded theory for analysis and processing, and, for grayscale images, it yields a nonlinear method for geometry-based processing.

The principal morphological representation for *binary images* is the *skeleton* [19, 21, 28]. The skeleton (defined below) was originally proposed and developed independently of mathematical morphology, and is sometimes still used today with no aid from the morphological theory (e.g., see [31]). On the other hand, it was proved that the skeleton can be calculated entirely by the basic operations of mathematical morphology [19], which makes the skeleton a morphological representation, enabling image analysis using morphological tools.

Blum [2] introduced the notion of skeleton by means of the following intuitive model: Suppose a given shape to be a grass field, and suppose that at time $t = 0$ its whole boundary is set on fire. The fire then propagates inwards at a constant speed. The set of points at which the fire extinguishes is the skeleton of the shape.

Since its intuitive introduction, the skeleton has been defined mathematically in a number of ways. The various definitions are different characterizations of the "Grass-fire" model, and they provide (almost) equivalent results for continuous planar shapes. A common definition of the skeleton is the following [27]:

Definition 1 *Let a* maximal disc *inscribable in a given shape $X \subset \mathcal{R}^2$ be a disc included in X, but not contained in any other disc included in X.*

The skeleton of X is the set of centers of all its maximal discs.

Fig. 1 illustrates the above definition.

As noted by Serra [29], the morphological skeleton theory has developed in the literature in both topological and algebraic branches. From the topological point of view, the skeleton of a shape can be seen as a thin, topology-preserving caricature of the shape that is useful for image analysis and pattern recognition. From an algebraic point of view, the skeleton is the result of the *decomposition* of a given set into the superposition of simpler elements, selected from a pre-defined family of

elements (discs of increasing sizes). That decomposition provides an image *representation*, which consists of the collection of skeleton points, together with the radii of the corresponding maximal discs. The reconstruction of the original shape is obtained by the union of all the maximal discs. Since our main interest is in coding, this paper follows the algebraic branch.

Let us elaborate on the skeleton representation and its application to compression. The following are the main algebraic properties of the skeleton representation:

- The skeleton representation can be calculated by means of an algebraic closed-form formula, due to Lantuéjoul [19] (see also [27, 21]), which is reviewed in Section 2.

- The skeleton provides a decomposition of the original shape into features (discs) of different sizes, which can be seen as components in different "scales". The smallest maximal discs can often be considered as "detail", whereas the largest ones can often be considered as the main (coarse) structure. This provides a *hierarchical* or *pyramidal* interpretation to the skeleton representation.

- Simplified (morphologically "low-pass" filtered) versions of the original shape are obtained by partial reconstructions from the skeleton representation (see Fig. 2).

The skeleton representation has the following undesired characteristics:

- It usually contains *redundant points*, that is, many skeleton points can be discarded and still the original shape can be fully reconstructed (see Fig. 3). The redundant points usually form long, undesired, branches in the skeleton. Mathematical characterization of the redundant points can be found in [13], and methods for redundancy reduction are proposed in [21, 22, 13, 15].

- Unlike other image representations (e.g., chain code and quadtree), it is not a self-dual representation, because the skeleton of X^c (the complement of X) is totally different from the skeleton of X (see [10] for background on self-dual operators).

The skeleton representation can be considered as a low-complexity, sub-optimal solution to the following problem:

Problem 1 *Let $\{\mathcal{F}_i\}$ be the family of all discs (with all sizes and positions).*

For any given shape X, what is the smallest subset of $\{\mathcal{F}_i\}$ that exactly covers X?

It is a low-complexity solution due to the existence of a closed-form formula for the skeleton calculation; it is sub-optimal because it contains redundancy.

The above serves as a framework to skeleton-based coding of binary images. That framework has been applied not only to compression of original binary images, like facsimile [4] or sign-language sequences [21], but also in grayscale coding schemes in which binary images are extracted from the original one. For example, in [25], the bit-planes of a grayscale image, which are each a binary image, are coded by a skeleton decomposition. Another approach, which gained interest in recent years, is to use the skeleton to code the segment contours in the context of segmentation-based coding [33, 3, 8, 6].

However, the compression rates achieved until now by lossless coding of the skeleton are only comparable to (and sometimes even worse than) other simpler methods, such as chain coding, quadtree decomposition, or run-length/Huffman coding, applied directly to the original image. This is in spite the fact that the structure of the skeleton has been extensively studied and generalized in recent years [27, 21, 25, 26, 28, 29, 14], and several different coding schemes of the skeleton have been tried [21, 4, 3].

In this paper, we present a number of theorems introduced recently by the authors in [16] (see also [18]) concerning properties of the *discrete* skeleton representation of binary images. These properties, being new, are not used by previous skeleton-coders, and this is reflected in their unsatisfactory performance. By taking these properties into account, one can either considerably improve the previous schemes, or design efficient new ones.

One such new coding scheme, originally proposed by the authors in [17, 18], is also presented and compared to other algorithms. Computer simulations indicate that, typically, the proposed coding scheme substantially improves the coding rates obtained by one of the best previous schemes for skeleton coding, and is more efficient than coding the original image by chain code, quadtree and run-length/Huffman methods. For facsimile images, it usually performs better than the MR algorithm with $K = 4$ (used in the Group 3 standard – G3), but, at this point, it is weaker than the MMR algorithm (used originally in the Group 4 standard, G4, only, and adopted later in G3) and the JBIG standard [9].

This paper is organized as follows. Section 2 provides a theoretical background for the morphological skeleton representation. In Section 3, some previous coding schemes for the skeleton representation are briefly presented and compared. Section 4 reviews advanced concepts in mathematical morphology that are required in the sequel. The new skeleton properties are then presented

in Section 5, and the proposed scheme, using these properties, is presented in Section 6. Simulation results are shown in Section 7, generalizations and extensions are proposed in Section 8, and Section 9 concludes the paper.

2 Morphological Skeleton Representation

This section provides a theoretical background on the morphological skeleton representation. We assume reader familiarity with the basic binary morphological operators: dilation, erosion, opening, and closing (the definitions and properties of these operators can be found, for example, in [5, 27, 18]). Like in some of these references, the dilation, erosion, opening, and closing of a binary set X by a structuring element B are denoted here by $X \oplus B$, $X \ominus B$, $X \circ B$, and $X \bullet B$, respectively.

2.1 Skeleton Computation Via Morphological Operations

In [19] (see also [27]), Lantuéjoul proved that the skeleton $S(X)$ of a topologically open shape X in $\mathcal{R}^2$ can be calculated by means of binary morphological operations. In that context, the sets $S_r(X)$, $r > 0$, each containing the centers of the maximal discs of radius r, are calculated by means of Lantuéjoul's formula[1]:

$$S_r(X) = X \ominus rB - [(X \ominus rB) \circ drB], \tag{1}$$

where rB and drB denote, respectively, the topologically open disc with radius r and a topologically closed disc with infinitesimal radius dr, centered at the origin. The skeleton $S(X)$ is the union of all the sets $S_r(X)$, $r > 0$.

In (1), the set $X \ominus rB$ represents the portion of the "grass field" not yet burned by the fire, at time $t = r$, in the "grass-fire" model for the skeleton (see Section 1). By increasing r, one simulates the "fire propagation". The set $[(X \ominus rB) \circ drB]$ represents the points at which the fire does *not* extinguish at time $t = r$. Therefore, the difference between the above sets provide the skeleton points at $t = r$. Since the morphological opening by a disc with infinitesimal radius excludes from a shape its protruding vertices, one concludes that the skeleton points with radius r of a shape X are the protruding vertices of the "fire front" $X \ominus rB$ (see Fig. 4).

The sets $\{S_r(X)\}_{r>0}$ are called the *skeleton subsets*, and the function $q(s)$ relating to each skeleton point s the radius of the respective maximal disc is called *quench function* [27, 21].

[1] From the strict mathematical point of view, equation (1) is an informal version of the original Lantuéjoul's formula. The reader can refer to [19] or [27] for the original version.

From the collection of skeleton subsets one can obtain perfect or partial reconstructions of the original open shape X as follows:

$$X \circ qB = \bigcup_{r>q} S_r(X) \oplus rB, \tag{2}$$

where q is a non-negative scalar. For $q > 0$, the skeleton subsets with radii smaller than and equal to q are discarded, and a smooth version of X ($X \circ qB$) is obtained. By setting $q = 0$ in (2), one obtains a perfect reconstruction. That means that the collection of skeleton subsets $\{S_r(X)\}$ can be considered as a *representation* of the original set X.

2.2 Generalized-step Skeleton

The above morphological skeleton representation has been generalized several times in the last fifteen years with the purpose of extending the skeleton's scope and decomposition family. Serra presented a discretized version of Lantuéjoul's formula in [27], where the decomposition elements approximate discs of discrete radii in a grid. In [21], Maragos and Schafer suggested the use of decomposition elements other than discs, by appropriately replacing the structuring element in the discretized Lantuéjoul's formula. The theorems presented in Section 5 below are related to a further generalization, proposed by Maragos in [20, page 191] (see also [23]). It is referred to as the generalized-step skeleton in [26], and its definition is reviewed below. More recent generalizations, which are outside the scope of this paper, can be found in [29, 14, 18].

Let E be an Euclidean space ($\mathcal{R}^2$ in the continuous case, or $\mathcal{Z}^2$ in the discrete case), and let $\{B(n)\}_{n\in\mathcal{N}}$ be a series of topologically open structuring elements in E, each containing the origin. Moreover, let this series generate a family of elements $\{A(n)\}_{n\in\mathcal{N}}$ in the following way:

$$\begin{cases} A(0) = (0,0) \\ A(n+1) = A(n) \oplus B(n), \quad n = 0, 1, 2, \ldots \end{cases} \tag{3}$$

The family $\{A(n)\}$ generalizes the concept of "discs", used in the definition of skeleton (Definition 1). The discrete parameter n assumes here the role of the *radius* of the discs. As an example, $\{A(n)\}$ is the family of discrete squares of sides $2n + 1$ pixels, when $B(n)$ is set to the 3×3-pixel elementary square for all values of n.

The generalized-step skeleton decomposition is defined by (adapted from [20, 23], see also [26]):

$$S_n(X) = X \ominus A(n) - [X \ominus A(n)] \circ B(n), \qquad n = 0, 1, \ldots \tag{4}$$

The sets $S_n(X)$, $n \in \mathcal{N}$, and eq. (4) are considered as generalizations of the skeleton subsets and Lantuéjoul's formula (1), respectively. As a consequence of the work in [29] (see also [18]), it can be shown that indeed the subsets $\{S_n(X)\}$ are composed of the positions ("centers") of the maximal elements from the above family $\{A(n)\}$ inside the input image X. The above result applies both to continuous and discrete input images.

A reconstruction formula from the above skeleton, analogous to (2), is given by:

$$X \circ A(k) = \bigcup_{n \geq k} S_n(X) \oplus A(n), \tag{5}$$

where k is a non-negative integer. Perfect reconstruction is obtained for $k = 0$. That means that, like the original skeleton subsets, the generalized-step skeleton subsets also fully represent the original image X. We call the indices n the "radii" of the skeleton points, by analogy to the original skeleton. For example, see Fig. 7(a), where $\{A(n)\}$ is the same family of discrete squares as defined above.

Instead of decomposing X into the union of maximal *discs*, as in the original skeleton, a generalized-step skeleton decomposes X into the union of maximal elements of the more general increasing family $\{A(n)\}$. Note that the family of elements $\{A(n)\}$, used in the above skeleton decomposition, is indexed by *natural* numbers $(0, 1, \ldots)$. Therefore, we say that it is a "discrete-family" skeleton. On the other hand, notice that X and the shapes in the above decomposition family are not restricted to be discrete. They can be discrete (sets in $\mathcal{Z}^2$), or continuous (sets in $\mathcal{R}^2$).

For simplification, we adopt from this point on the following notation:

$$X_n \stackrel{\triangle}{=} X \ominus A(n), \tag{6}$$

$$Y_{n+1} \stackrel{\triangle}{=} X_{n+1} \oplus B(n) = [X \ominus A(n)] \circ B(n). \tag{7}$$

With the above notation, we can write the generalized Lantuéjoul's formula (4) in the following way:

$$S_n = X_n - Y_{n+1}. \tag{8}$$

3 Previous Coding Schemes

In this section we review some coding schemes for the skeleton representation proposed in the literature, and briefly discuss their characteristics. These schemes assume a constant generator, i.e. $B(n) = B$, $\forall n$, but they can be easily extended for any generalized-step skeleton.

In [21], Maragos and Schafer propose two different schemes. In the first one, the skeleton subsets S_n, $n = 0, 1, \ldots$, are considered as binary images, which are usually very sparse, and therefore suitable for very low bit-rate coding. Thus, each skeleton subset has its run-length coded by a Huffman or an Elias code. The skeleton subsets are coded in decreasing order of n, providing a *progressive transmission* scheme, since according to the partial reconstruction formula (5), if the decoding is halted at a certain point, a simplified version of the original image is obtained. However this coding method is inefficient because coding each skeleton subset independently does not take into account the strong correlation that exists between them.

The second scheme proposed in [21] consists of coding the binary image formed by the *union* of all skeleton points, $S \stackrel{\triangle}{=} \cup\{S_n\}$, plus the quench function $q(s)$, $s \in S$. The skeleton image S is coded as in the first scheme by run-length/Huffman or Elias code. The quench function is coded by a Huffman code. Compared to the first scheme, it is faster since it requires only one binary image to be scanned instead of scanning each skeleton subset separately. However, it does not permit progressive transmission. It is also inefficient in terms of coding because it neglects any correlation that might exist between the position of the skeleton points and their quench values. Recently, this approach has been extended for coding segment contours in the context of segmentation-based coding [3, 33] (we elaborate on that in Section 8).

The last algorithm we review here is proposed by Brandt, Jain, and Algazi in [4], and consists of chain coding the skeleton lines. The motivation is that, in the continuous case, the skeleton lines of connected shapes are almost always connected. To take advantage of this, it is proposed to code the skeleton lines by an extended chain code, with symbols indicating at each point if the related radius increases, decreases or is unchanged, in addition to the direction of the next point, and with a header for each skeleton line indicating the position and the radius of its first point. However, in the discrete case, as opposed to the continuous case, the skeleton lines may have many gaps, and this considerably reduces the efficiency of chain coding.

A redundancy-reduction algorithm is usually performed in order to remove most or all the redundant points in the skeleton (see [21, 13]). This improves considerably the efficiency of the first two schemes, but the correlation is still not taken into account. Moreover, the removal of redundant points breaks even more the continuity of digital skeleton lines, and this reduces by a great deal the performance of the last scheme. On the other hand, artificially connecting the broken lines of the digital skeleton, by using dummy skeleton points (aiming to improve the efficiency of the last scheme), increases the number of redundant points in the skeleton. A trade-off between

connectivity and redundancy removal is therefore created and the preferred approach is not clear.

4 Some Advanced Concepts in Binary Morphology

The concepts of descendance, connectivity, reconstruction, and ultimate erosion are fundamental ones in this work. They are reviewed in the following subsections, and some of them are slightly modified for our needs. Also, this section introduces part of the notation used in the sequel.

4.1 Descendance and Connectivity

The definitions of descendance and connectivity presented here are adapted from [28, pages 77 and 78].

Definition 2 (Direct Descendance) *Let B be a structuring element contained in E. A point $y \in E$ is a* direct descendant *of a point $x_0 \in E$, under the given structuring element, iff:*

$$y \in \{x_0\} \oplus B. \tag{9}$$

Definition 3 (Descendance) *A point $y \in E$ is a* descendant *of a point $x_0 \in E$, under the given structuring element, iff there is a chain of points, each being a direct descendant of a previous one, starting with x_0 and ending with y.*

Definition 4 (Connectivity) *Two points x_0 and y are connected (under a pre-defined structuring element B) iff each one is a direct descendant of the other, under B, i.e.:*

$$x_0 \in \{y\} \oplus B \text{ and } y \in \{x_0\} \oplus B. \tag{10}$$

Intuitively, B defines a *neighborhood* for which descendance and connectivity are considered. A point descends directly from another if the former belongs to the neighborhood of the latter. Similarly for connectivity. If, moreover, B is *symmetric* (i.e., $b \in B \Rightarrow -b \in B$), then y is a direct descendant of x_0 iff x_0 is a direct descendant of y. Therefore, in this case, direct descendance and connectivity are equivalent.

4.2 Reconstruction Operator

Reconstruction is an important morphological operator, which finds use in several applications, such as extraction of connected components and filtering [30]. It should not be confused with the

reconstruction of the original image X from its skeleton representation, considered in the previous sections. The reconstruction operator is defined as follows.

Definition 5 (Reconstruction) *Let A, D be two sets in E, such that $D \subseteq A$, and B be a pre-defined structuring element. The* reconstruction *of A from D under B, $Rec\{A, D\}_B$, returns the set of points in A that descend from points in D, under B, through a path of points strictly in A.*

When B is a *symmetric* structuring element, the reconstruction of A from D is the collection of *connected components* of A that contain points of D (see Fig. 5).

One way of performing the reconstruction operation is by recursively calculating a *conditional dilation*. Specifically, if $\delta_{A,B}(D) \stackrel{\triangle}{=} (D \oplus B) \cap A$, and $\delta^n_{A,B}(\cdot)$ denotes the n-fold application of $\delta_{A,B}(\cdot)$, then:

$$\mathrm{Rec}\{A, D\}_B = \lim_{n \to \infty} \delta^n_{A,B}(D). \tag{11}$$

Notice that the notion of connected component depends on the structuring element B chosen in the definition of connectivity. If it is too "big", then relatively distant points can eventually be considered connected. Therefore, B is usually selected to be as small as possible (an 8-pixel or 4-pixel neighborhood, in the discrete case, or a infinitesimally small disc in the continuous case).

4.3 Ultimate Erosions

In [27], the *ultimate erosions* are defined in terms of a decreasing family of erosions $\{X \ominus nB\}$, where n is a natural number, and nB denotes the n-fold dilation of B by itself. For each n, the ultimate erosions of order n, denoted U_n, of a given set $X \subset E$, are defined by:

$$U_n \stackrel{\triangle}{=} X \ominus nB - \mathrm{Rec}\left\{X \ominus nB, [X \ominus nB] \circ B\right\}_B. \tag{12}$$

In words: The ultimate erosions of order n are the points of $X \ominus nB$ that do not descend, under B, from the opening of $X \ominus nB$ by B.

Intuitively, the ultimate erosions, at each erosion step, mark the "convex sub-regions" of X that are about to disappear after a further erosion. Fig. 6 shows an example, with B being a disc. Notice that, although the original set X is composed of two connected components, the ultimate erosions consist of three connected components, because one of the components of X is a union of two "convex sub-regions".

Here, we adapt the definition of ultimate erosions for generalized-step families as well:

Definition 6 *We define the ultimate erosions U_n as:*

$$U_n \stackrel{\triangle}{=} X_n - Rec\{X_n, Y_{n+1}\}_{C(n)}\,, \tag{13}$$

where X_n and Y_{n+1} are as defined in (6) and (7), respectively, and:

$$C(n) = \begin{cases} B(n-1), & n \geq 1, \\ Any\ structuring\ element, & n = 0. \end{cases} \tag{14}$$

The ultimate erosions as defined above *are contained in the generalized-step skeleton of X*, when the same family $\{A(n)\}$ is used in the computation of both the ultimate erosions and the generalized-step skeleton. This is because the result of the reconstruction operation in (13) contains the set Y_{n+1}, which is subtracted from X_n in the generalized Lantuéjoul's formula (4).

In practice, the ultimate erosions are those skeleton points with maximal "radius" within each "convex sub-region" of the original shape. They are usually a small percentage of the skeleton. For example, consider the image in Fig. 7(a), and its skeleton, calculated with a constant generator $B(n) = B$, equal to a 3×3 square structuring element. Fig. 7(b) shows its ultimate erosions, which belong in this case to U_2 and U_3 only. Fig. 8, shows another example, where the skeleton is calculated using the same decomposition family of squares as in the first example.

5 New Skeleton Properties

Our main theoretical results concerning coding are presented in this section. They are related *only* to **discrete-family** generalized-step skeleton representations (see Section 2.2).

The theoretical results are new skeleton properties, divided into two categories: Quench-function sampling, and deterministic prediction.

5.1 Quench-Function Sampling

In this subsection, we show that, for a *discrete-family* generalized-step skeleton, one can discard the "radius" of most of the skeleton points from the representation, and still perfect reconstruction is possible. More specifically, the radii of the points that do not belong to the ultimate erosions can be discarded!

The following lemma helps us formulate the above assertion in the form of a theorem.

Lemma 1 *Let $\{S_n\}_{n\in\mathcal{N}}$ be the skeleton subsets of a generalized-step skeleton, and let S be the set of skeleton points, carrying no information about the radii; that is, $S \stackrel{\triangle}{=} \bigcup_{n\geq 0} S_n$. Then, the following holds:*

$$Rec\,\{S \cup Y_{n+1}, Y_{n+1}\}_{C(n)} \cup U_n = X_n. \tag{15}$$

The above result is used in the proof of the next theorem, and leads to the corollaries presented below. The proof of Lemma 1 is given in the Appendix.

The following theorem is the main result in this section.

Theorem 1 *Let $\{S_n\}_{n\in\mathcal{N}}$ be the generalized-step skeleton subsets of a given image X, and $S \stackrel{\triangle}{=} \bigcup_{n\geq 0} S_n$. Let ultimate erosions be defined as in (13).*

Then X is completely represented by the sets $\{U_n\}_{n\in\mathcal{N}}$ and S.

In other words, the radii of the skeleton points that are ultimate erosions, together with the position of all the skeleton points, are sufficient for completely representing the original set X.

Proof *We use induction in the following way:*

1. *If N is the maximal radius in the skeleton, then $X_N = U_N$.*
2. *For each n, $N > n \geq 0$, once X_{n+1} is known, the set X_n can be calculated (see below), and*
3. *the original image X is equal to X_0.*

In order to obtain the second part of the above induction, suppose that X_{n+1} is available. Therefore Y_{n+1} is also available. From the hypothesis, the skeleton S and the ultimate erosions $\{U_n\}$ are provided. Then X_n is obtained from the above by Lemma 1. □

The above proof is constructive; it provides a reconstruction algorithm for the original image from the resulting "sampled" skeleton. It consists of calculating at each step n, which varies from N down to 0, the set X_n according to (15). This can be implemented in the following way (illustrated by Fig. 9):

1. An intermediate image, which we call Z, is created and initially set to the highest ultimate erosions, i.e., $Z = U_N$.
2. $n \leftarrow N - 1$. (We assume $N \geq 1$, otherwise, we trivially obtain $X = U_N$).

3. $Z \leftarrow Z \oplus B(n)$. At this point Z is equal to Y_{n+1}. According to Lemma 1, for a symmetric $C(n)$, S_n is the set of those connected components of S that "touch" Z, in addition to the ultimate erosions U_n (see Fig. 9).

4. $Z \leftarrow \mathrm{Rec}\{S \cup Z, Z\}_{C(n)} \cup U_n$. According to Lemma 1, at this point Z is equal to X_n. Note that the points appended to Z in this step are those of S_n.

5. If $n = 0$, stop, and $X = Z$. Otherwise, $n \leftarrow n - 1$.

6. Go to step 3.

The above algorithm is also the heart of the coding scheme proposed in Section 6.

The following corollaries are a direct consequence of (15).

Corollary 1 *If s is a skeleton point with radius n, then all the skeleton points that descend from it, under $C(n)$, have also radius n.*

Corollary 2 *Suppose that $C(n)$ is* symmetric, *i.e., $c \in C(n) \Rightarrow -c \in C(n)$.*

In this case, if s is a skeleton point with radius n, then all the skeleton points in the connected component to which it belongs (with connectivity being under $C(n)$) have also radius n.

Corollary 2 can be seen as a generalization of property 3.2 in [4], which states that the radius (called "distance value" there) of each connected component is constant, when the structuring element is a 3×3 square.

According to the above corollaries, not even all the ultimate-erosion points need to have their radius stored! In the case of symmetric decomposition elements, corollary 2 states that, for every connected component in the set of ultimate erosions, one needs to store only the radius of *one point*. Note that the set of ultimate erosions is usually a very small subset of the skeleton points, and, due to the above consideration, only a small percentage of them need to have their radius stored. Similar results can be deduced for non-symmetric decomposition elements, by means of Corollary 1. The above observations lead to an improved sampling scheme of the quench function (see Fig. 10).

Corollary 3 *A skeleton point s has radius n* if and only if *s belongs to U_n,* **or** *$s \notin Y_{n+1}$ but s descends from Y_{n+1}, under $C(n)$.*

The above corollaries are used in the coding scheme proposed in Section 6.

5.2 Deterministic Prediction

The second theorem on which the proposed scheme is based is presented below. It permits *deterministic prediction* of information about S_n from the knowledge about the previously coded points.

Suppose a coding procedure where, at a certain step, the skeleton subset of order n, S_n, is to be coded, and that Y_{n+1} is known to both the encoder and the decoder. Since $S_n = X_n - Y_{n+1}$, it follows that there are no points of S_n inside the region Y_{n+1}. Therefore the encoder does not need to code the *status* (whether belonging, or not, to S_n) of the pixels inside Y_{n+1}, and the decoder does not need to "look for" skeleton points in that region at that moment. This result was used in the coding schemes proposed in [21].

It turns out that there is also a region *outside* Y_{n+1} that can be predicted not to contain skeleton points from S_n. This region can be characterized by the following theorem:

Theorem 2 *Let $p \in E$. If the following holds:*

$$[(Y_{n+1} \cup \{p\}) \bullet A(n)] \circ B(n) \supset \{p\}, \tag{16}$$

then p cannot belong to S_n.

Proof *The proof is by contradiction. Suppose that p is in S_n, and let us define the following operator:*

$$\rho(Z) \stackrel{\triangle}{=} [Z \ominus A(n)] \circ B(n). \tag{17}$$

By definition of Y_{n+1} in (7), $\rho(X) = Y_{n+1}$. In addition, operating $\rho(\cdot)$ on the set $Y_{n+1} \oplus A(n)$ also results in Y_{n+1}, since:

$$\begin{aligned} &[(Y_{n+1} \oplus A(n)) \ominus A(n)] \circ B(n) = \\ &\quad = \; X \ominus A(n+1) \oplus B(n) \oplus A(n) \ominus A(n) \ominus B(n) \oplus B(n) \\ &\quad = \; \{[X \circ A(n+1)] \ominus A(n+1)\} \oplus B(n) = [X \ominus A(n+1)] \oplus B(n) = Y_{n+1}. \end{aligned} \tag{18}$$

Therefore, since $\rho(\cdot)$ is an increasing operation (it is composed of basic morphological operations, which are increasing), then any set Z_0, such that $[Y_{n+1} \oplus A(n)] \subseteq Z_0 \subseteq X$, satisfies $\rho(Z_0) = Y_{n+1}$. In particular, $Z_0 = (Y_{n+1} \cup \{p\}) \oplus A(n)$, $p \in S_n$, satisfies it.

However, according to (16), $\rho(Z_0) \supset \{p\}$, and, therefore, $p \in Y_{n+1}$, which contradicts that $p \in S_n$. □

Theorem 2 provides a test for each point p in E: If it passes it, i.e. if (16) holds, then its status as a skeleton point needs not to be coded because it is known to both encoder and decoder to be negative. On the other hand, if the test fails ((16) does not hold), nothing can be said about the status of that point, and it must be coded.

The above test is however not viable in practice, because it is extremely computation-intensive. Luckily, a simplified, much faster test is possible in many cases using the following corollary:

Corollary 4 *Let F be a structuring element,* not containing the origin *(which we denote by o), and satisfying:*

$$[(F \cup \{o\}) \bullet A(n)] \circ B(n) \supset \{o\}, \tag{19}$$

and let $p \in E$.

If $\{p\} \oplus F \subseteq Y_{n+1}$, then p cannot belong to S_n.

In other words, one can pre-select a template F, excluding the origin, and usually containing a small number of points, such that it satisfies (19). Since it is independent of the input image X, the above selection is done "off-line", and only once for a given decomposition family $\{A(n)\}$. During an "on-line" coding algorithm, the "prediction test" is performed, for each point p, by placing F "on" p, and examining the status of the points indicated by the template.

The points found in the above test are only a *subset* of the "predictable points" found in the test of Theorem 2. In order to find *all* the predictable points, a family $\{F_i\}$ of *all* the templates satisfying (19) should be defined, and the test in Corollary 4 must be repeated for each F_i. This could also be very computation-intensive. It turns out, however, (from simulations) that often a small subset of $\{F_i\}$ is enough for finding *most* of the predictable points. As an example, let $E = \mathcal{Z}^2$, and consider a skeleton decomposition of X, where $B(n) = B$, $\forall n$, and B is a 3×3-*pixel square structuring element.* In this case, Corollary 4 above for $n > 0$ can assume the following specific format:

Corollary 5 *Suppose $n > 0$, let $(i, j) \in \mathcal{Z}^2$, and consider a morphological skeleton with a 3×3-pixel* square *structuring element. If any of the triplets*

$$\{(i + k_1, j), (i, j + k_2), (i + k_3, j + k_3)\},$$
$$\{(i - k_1, j), (i, j - k_2), (i - k_3, j - k_3)\},$$
$$\{(i + k_1, j), (i, j - k_2), (i + k_3, j - k_3)\},$$
$$\{(i - k_1, j), (i, j + k_2), (i - k_3, j + k_3)\},$$

for any integers k_1, k_2 and k_3 in the interval $[2, 2n+1]$, is contained in Y_{n+1}, then the point (i, j) does not belong to S_n.

The above triplets represent a subset of the family $\{F_i\}$ related to the given squared structuring function. Fig. 11 shows an example of a point (i, j) that is predicted not to belong to S_n in this specific case. Fig. 12 shows another example; in this case, $n = 1$, and Y_{n+1} is indicated by the thick line. The dark points are those that can be predicted *not* to belong to S_1, according to Corollary 5.

6 Proposed Coding Scheme

The properties proved in Section 5 can be used to either substantially improve the coding schemes reviewed in Section 3, or to design new ones. For instance, the first scheme by Maragos and Schafer reviewed in Section 3 (coding of $\{S_n\}$) could directly benefit from deterministic prediction, whereas the second one (coding of S plus the quench function) could directly benefit from quench-function sampling. Another expected improvement for the first algorithm would be to move all the non-ultimate-erosion skeleton points from their original subsets to the same subset, e.g., S_0. The algorithm by Brandt, Jain, and Algazi could be also improved by avoiding transmission of the radii of the non-ultimate-erosion skeleton points. However, despite the expected improvement, the above modifications do not exhaust the benefits of the new properties.

In this section we propose a new coding scheme of the skeleton representation of binary images. It gathers most of the advantages of each of the above algorithms, besides fully benefiting from the new theoretical properties. It is progressive like the first algorithm by Maragos and Schafer, fast as the second one, and explores the connectivity present in the skeleton like the algorithm by Brandt, Jain, and Algazi. As a consequence of the above, the proposed scheme gives better results in simulations for compression of binary images than the previous schemes (see Section 7 below).

The coding scheme proposed here is restricted to discrete-family generalized-step binary skeletons, defined on $\mathcal{Z}^2$ (discrete binary images).

6.1 The Algorithm

After the generalized-step skeleton representation is calculated, the coding is performed in the same way as the decoding, i.e., by reconstructing the original image. Let N be the maximal radius.

Initially, for each of the ultimate erosions U_n, $0 \leq n \leq N$, a set $\tilde{U}_n$ is formed, in such a way that if a point s belongs to $\tilde{U}_n$, then it does not descend from any other point in $\tilde{U}_n$, under $C(n)$. If

$C(n)$ is symmetric, the above means that $\tilde{U}_n$ contains only one point of each connected component of U_n, under $C(n)$. The points in the sets $\tilde{U}_n$ have their positions and radii coded. The choice of the specific coding method for the above operation is not critical, since the amount of information that is conveyed by the sets $\{\tilde{U}_n\}$ is usually a small fraction of the overall information in the image. In our simulations, we coded the pixels of $U \stackrel{\triangle}{=} \bigcup_n U_n$ and the corresponding radii, separately, with an arithmetic coder.

At this point, the main loop starts. At each step n, which varies from its maximum value, N, down to 0, a scanning procedure is performed on the *external boundary* of Y_{n+1} and of $\tilde{U}_n$. The external boundary of a set A is considered here to be the points outside A that are direct descendants of points in A, under $C(n)$.

Only the external boundary has to be searched for points in S_n, since the skeleton points in S_n are necessarily linked either to Y_{n+1}, if it is not an ultimate erosion point, or to $\tilde{U}_n$, otherwise, according to Corollary 3. Some points in the above scan can be predicted not to belong to S_n by the test in Theorem 2; these points are skipped. The skeleton points found in the above scan *must* belong to S_n (according to the reconstruction algorithm related to Theorem 1), and their relative positions in the scanning path are coded by an arithmetic coder [11]. When a skeleton point is found, its boundary is searched for other connected skeleton points in a recursive way, before the main scanning procedure goes on.

In simulations, we found it very beneficial to use *two* separate *adaptive probability models* for the arithmetic coder. A *probability model* is the collection of the probabilities of appearance of each of the symbols to be coded. In an *adaptive* model, the probabilities are updated after each input symbol is coded[2]. One adaptive model is used for coding the position of points in the main scan, whereas the second adaptive model is used for coding the position of points that are adjacent to previously found skeleton points (local scan).

The whole coding procedure is detailed in the following algorithm:

1. Calculate the skeleton subsets S_n, $0 \leq n \leq N$. Form and code the sets $\tilde{U}_n$ as specified above.

2. $n \leftarrow N-1$. $Y_N \leftarrow \emptyset$.

3. $Z \leftarrow (Y_{n+1} \cup \tilde{U}_n)$.

[2]In the empirical adaptive model used in this work, the probabilities for the symbols "0" and "1" are initially set to 0.5, and, during the coding process, updated to $m_i/(m_0+m_1)$, where m_i-1 is the number of previous appearances of the symbol i, $i = 0, 1$.

4. $p \leftarrow$ (an external boundary point of Z). If there are no more external boundary points to scan, go to step 9.

5. Check (by means of Theorem 2) if p can belong to S_n or not. If it cannot, go to step 4.

6. Send to the arithmetic coder a "0" if p is not a skeleton point or a "1" otherwise. Use an adaptive probability model.

7. If a "1" was sent (i.e., p is a skeleton point), then $Z \leftarrow (Z \cup \{p\})$. Otherwise, go to step 4.

8. Recursively, scan the direct descendants of p for other connected skeleton points. Code non-predictable points with "0" or "1" accordingly, but use a different adaptive probability model than the one in step 6. After the whole connected component is scanned and coded, go to step 4.

9. If $n = 0$, stop.

10. $n \leftarrow (n-1)$. $Y_{n+1} \leftarrow Z \oplus B(n)$. Go to step 3.

6.2 Discussion on Redundancy Removal

As pointed out in Sections 1 and 3, there are usually redundant points in the morphological skeleton representation, which can be removed (together with their radii) from the representation without affecting its error-free characteristic. This should not be confused with the result, presented in this paper, that non-ultimate-erosion points can have their *radii* (only) removed from the representation, while keeping the representation complete. Actually, the two kinds of points (redundant and ultimate erosion ones) are not related, and there can be redundant ultimate erosion points as well as non-ultimate erosion points which are not redundant.

Unfortunately, one can not usually use both properties, i.e., to remove the redundant points *and* the radii of non-ultimate erosion points. That is because the removal of redundant points may disconnect connected components of the skeleton, and the existence of the connectivity is crucial for proving Theorem 1 presented here. This means that, after redundancy removal, Theorem 1 may not remain valid. For this reason, the theoretical results and the algorithm presented in the previous sections a priori assume no redundancy removal.

However, there are two ways to modify the above situation. One is to perform a redundancy reduction that preserves connectivity (e.g., the scheme presented in Section 6.3 below). The second way is to appropriately add new points to the list of ultimate erosions. Details and implementation

of the latter are outside the scope of this paper, but Section 8 below briefly describes and comments about it.

6.3 Coding With the Square Structuring Element

A particular redundancy reduction scheme, suitable only for the skeleton with the 3×3 square structuring element, is proposed here. It removes a large fraction of the redundant points, without affecting the connectivity. In this case, one can benefit both from redundancy reduction and quench-function sampling.

The redundancy reduction scheme consists of *sequentially* discarding points of the skeleton, with radius greater than 0, for which at least 3 out of the 4 closest neighbors are also skeleton points. Fig. 13 demonstrates the result of applying the scheme in a simple image, where part of the skeleton belongs to S_1 and part to S_2. Note that the representation remains error-free.

7 Simulation Results

The simulations of the proposed scheme presented here correspond to a skeleton with a constant generator $B(n) = B$, equal to the 3×3 squared structuring element centered at the origin. This particular structuring element was chosen so that Corollary 5 and the special redundancy algorithm presented in Section 6.3 can be used. Moreover, $C(0) = B$.

Two sets of simulation tests are presented.

The first one compares the lossless compression efficiency of the algorithm proposed in Section 6.1 with some simple, well-known coding schemes for binary images. The test image is the 256×256-pixel "Tools" (Fig. 14). The results, in bits/pixel, of the comparison are presented in Table 1. As seen from the table, the proposed skeleton coder provides the best compression (only 0.071 bits/pixel).

The second set of simulation tests examines the efficiency of the proposed skeleton coder in coding scanned documents (fax), and compares it to existing standard coders [1, 9]. A previous skeleton-based scheme proposed in [4] (denoted d_8 skeleton) is also compared. The eight CCITT facsimile standard test 2376×1728-pixel images, of documents scanned at 200 dpi, are losslessly coded by the proposed algorithm. Table 2 compares the size of the obtained coded files with the results given in [1] and [4]. Comparison of our results to the d_8 skeleton shows a substantial improvement in skeleton-based coding. At this point, it is still weaker than the most advanced

standards (G4, using the MMR algorithm, and JBIG), but it is comparable to the G3 standard (using the MR algorithm, with $K = 4$), being usually more efficient than it (with exception of the "hardest" images, #4 and #7).

Since the scanning in the algorithm is performed *on the boundaries* of the expanding set Z only (Section 6.1), the encoding and the decoding procedures are relatively fast. On a Digital DECStation 5000 (approximately 27 MIPS), programmed in standard C, encoding of the 256×256-pixel image "tools" takes about 4 seconds, and its decoding about 2 seconds.

8 Generalizations and Extensions

Grayscale images. One continuation of this work deals with grayscale image coding using a generalization of the morphological skeleton representation to grayscale images (see [18, chapter 8]). The new theoretical results, presented here for binary images only, are extended there to the grayscale case, and the generalization of the proposed coding scheme is described.

Geodesic skeletons. As noted in the Introduction and in Section 3, skeleton representations have been investigated recently in the context of segmentation-based coding (see [33, 3]). In that specific context, segment contours are represented by either one of two special types of skeletons, called geodesic and overlapping skeletons. These skeletons assure that the contour lines that separate two adjacent segments are not represented twice. In [3], coding schemes for the geodesic skeleton of segment contours are considered. Unfortunately, neither the geodesic nor the overlapping skeleton are particular cases of the generalized-step skeleton, which means that, presently, the new properties and the coding scheme proposed here are not directly applicable in that context. Therefore, as already suggested in [33], future research should also concentrate on extending the results of this work to geodesic and overlapping skeletons, so that the proposed algorithm can be used in coding of segment contours.

Redundancy reduction. As mentioned in Section 6.2, the proposed algorithm can support the removal of redundant points also if one appropriately modifies the list of ultimate erosions (see details in [18, chapter 8]). The main idea behind this modification is to have new skeleton points added to the ultimate erosions in order to compensate for breaks in connectivity. A comparison between the original and the modified scheme brings us to the same connectivity vs. redundancy trade-off mentioned in Section 3. The trade-off is expressed in this case by the number of points in the "ultimate erosion list" vs. the number of redundant points in the

representation, and the preferred approach is still not clear.

9 Conclusion

Although very attractive from the theoretical point of view, skeleton-based coding of binary images has exhibited disappointing results in the past, since simpler coding schemes, like chain coding of the original binary image, showed similar (or even better) compression results. On the other hand, the skeleton coding schemes used in the previous experiments have not taken into consideration the strong correlation existing between skeleton subsets. Actually, this correlation was not properly characterized, and it was not clear how to efficiently use it.

In this paper, new theoretically-based properties characterizing the above correlation are presented, and a binary image coding scheme taking them into consideration is proposed.

The proposed binary coding scheme showed, in simulations, substantial improvement in the skeleton-based compression efficiency, as compared to one of the best previous skeleton-based coding schemes, and better results than those presented by the classical coding methods, including chain coding. When dealing with facsimile images (fax), the proposed coding-scheme is found to have similar performance to the MR coder used in ITU-T fax standards, but as yet is less efficient than the MMR and JBIG algorithms.

The scheme can be extended to grayscale images and redundancy-reduced skeletons, and seems to be extendible also to geodesic and overlapping skeletons. In addition, we believe that much can still be done to improve the efficiency of skeleton-based coding, especially in terms of statistical prediction and context classification.

Acknowledgment

The authors would like to thank the anonymous reviewers for their useful and thorough comments, which helped to improve the style and structure of the paper.

A Proof of Lemma 1

Let us define:

$$\begin{aligned} R_n &\stackrel{\triangle}{=} \mathrm{Rec}\{S \cup Y_{n+1}, Y_{n+1}\}_{C(n)} = \mathrm{Rec}\{S \cup S_n \cup Y_{n+1}, Y_{n+1}\}_{C(n)} \\ &= \mathrm{Rec}\{S \cup X_n, Y_{n+1}\}_{C(n)}. \end{aligned} \tag{A.1}$$

We note that:

$$\mathrm{Rec}\{S \cup X_n, Y_{n+1}\}_{C(n)} \supseteq \mathrm{Rec}\{X_n, Y_{n+1}\}_{C(n)} = X_n - U_n. \tag{A.2}$$

Therefore:

$$R_n \cup U_n \supseteq X_n. \tag{A.3}$$

On the other hand:

$$\mathrm{Rec}\{S \cup X_n, Y_{n+1}\}_{C(n)} \subseteq \mathrm{Rec}\{S \cup X_n, X_n\}_{C(n)}. \tag{A.4}$$

And we shall show that:

$$\mathrm{Rec}\{S \cup X_n, X_n\}_{C(n)} = X_n, \tag{A.5}$$

which gives, together with (A.4):

$$R_n \subseteq X_n. \tag{A.6}$$

Let us prove (A.5).

For $n = 0$, (A.5) holds trivially, since $X_0 = X$ (the original image), and $S \subseteq X$.

Suppose, therefore, $n > 0$. We have:

$$\begin{cases} X_n \oplus C(n) = X_n \oplus B(n-1) \\ [X_n \oplus B(n-1)] \cap S_{n-1} = Y_n \cap S_{n-1} = \emptyset \end{cases} \tag{A.7}$$

Which leads to:

$$[X_n \oplus C(n)] \cap S_{n-1} = \emptyset. \tag{A.8}$$

Similarly,

$$[X_n \oplus C(n)] \cap S_m = \emptyset, \quad \forall m < n. \tag{A.9}$$

Therefore, since $S_m \subseteq X_n$ for all $m \geq n$, we get:

$$[X_n \oplus C(n)] \cap [X_n \cup S] = X_n. \tag{A.10}$$

The conclusion is the validity of equation (A.5).

Now, from (A.3) and (A.6), we get $R_n \cup U_n = X_n$, which proves the Lemma.

References

[1] R. Aravind, G.L. Cash, D.L. Duttweiler, H. Hang, B.G. Haskell, and A. Puri, "Image and Video Coding Standards", *AT&T Technical Journal*, pp. 67-88, Jan./Feb. 1993.

[2] H. Blum, "A Transformation for Extracting New Descriptors of Shape", in *Models for the Perception of Speech and Visual Forms*, W. Wathen-Dunn Ed., Cambridge, MA: M.I.T. Press, 1967.

[3] P. Brigger, *Morphological Shape Representation Using the Skeleton Decomposition: Application to Image Coding*, D.Sc. thesis, École Polytechnique Fédérale de Lausanne, Swiss, 1996.

[4] J.W. Brandt, A.K. Jain and V.R. Algazi, "Medial Axis Representation and Encoding of Scanned Documents", *JVCIR*, Vol. 2, No. 2, pp. 151-165, June 1991.

[5] E.R. Dougherty, *An Introduction to Morphological Image Processing*, SPIE Volume TT 9, Washington, 1992.

[6] M. Van Droogenbroeck, *Traitment D'images Numériques au moyen D'algorithmes Utilisant la Morphologie Mathématique et la Notion D'objet: Application au Codage*, D.Sc. thesis (in French), Centre de Morphologie Mathematique, Fontainebleau, France, May 1994.

[7] C.R. Giardina and E.R. Dougherty, *Morphological Methods in Image and Signal Processing*, Prentice Hall, Englewood Cliffs, 1988.

[8] C. Gu, *Multivalued Morphology and Segmentation-Based Coding*, D.Sc. thesis, École Polytechnique Fédérale de Lausanne, Swiss, 1995.

[9] H. Hampel et al. , "Technical Features of the JBIG Standard for Progressive Bi-Level Image Compression", *Signal Processing: Image Communication*, Vol. 4, pp. 103-111, 1992.

[10] H.J.A.M. Heijmans, "On the Construction of Morphological Operators Which are Selfdual and Activity-Extensive", *Proc. Int'l. Workshop on Mathematical Morphology*, Barcelona, pp. 82-88, May 1993.

[11] P.G. Howard and J.S. Vitter, "Arithmetic Coding for Data Compression", *Proceedings of the IEEE*, Vol. 82, No. 6, pp. 857-865, June 1994.

[12] R. Kresch and D. Malah, "Two-Sided Skeleton - A Representation Composed of Both Positive and Negative Morphological Elements", *Proc. Int'l. Workshop on Mathematical Morphology*, Barcelona, pp. 145-150, May 1993.

[13] R. Kresch and D. Malah, "Morphological Reduction of Skeleton Redundancy", *Signal Processing*, Vol. 38, pp. 143-151, Sept. 1994.

[14] R. Kresch and D. Malah, "Multi-Parameter Skeleton Decomposition", *Proc. of the Int'l. Symp. on Mathematical Morphology ISMM'94*, J. Serra and P. Soille (eds.), pp. 141-148, Sept. 1994.

[15] R. Kresch and D. Malah, "Skeleton Redundancy Reduction Based on a Generalization of Convexity", *EUSIPCO-94*, Edinburgh, pp. 848-851, Sept. 1994.

[16] R. Kresch and D. Malah, "An Efficient Coding Scheme for Binary Images Based on the Morphological Skeleton Representation", *Proc. IEEE 18th Convention of Electrical and Electronics Engineers in Israel*, Tel Aviv, pp. 2.2.3/1-5, March 1995.

[17] R. Kresch and D. Malah, "New Morphological Skeleton Properties Leading to Its Efficient Coding", *IEEE Workshop on Non-Linear Signal and Image Processing 1995*, Neos Marmaras, Halkidiki, Greece, pp. 995-999, June 1995.

[18] R. Kresch, *Morphological Image Representation for Coding Applications*, D.Sc. Thesis, Department of Electrical Engineering, Technion, Israel, June 1995. Available at `http://www-sipl.technion.ac.il/publications/thesis/renato/renato.html`.

[19] C. Lantuéjoul, *La Squelettisation et son application aux mesures topologuiques des mosaiques polycristallines*, Theses de Docteur-Ingenieur, School of Mines, Paris, France, 1978.

[20] P. Maragos, "A Unified Theory of Translation-Invariant Systems with Applications to Morphological Analysis and Coding of Images," Ph.D. dissertation, School of Elec. Eng., Georgian Inst. Technol., Atlanta, U.S.A., July 1985.

[21] P. Maragos and R.W.Schafer, "Morphological Skeleton Representation and Coding of Binary Images", *IEEE Trans. ASSP*, Vol.34, No.5, pp. 1228-1244, Oct. 1986.

[22] P. Maragos, "Pattern Spectrum and Multiscale Shape Representation", *PAMI*, Vol.11, No.7, pp. 701-716, July 1989.

[23] P. Maragos, "Morphological Systems for Multidimensional Signal Processing," *Proc. of the IEEE*, Vol. 78, No. 4, pp. 690-710, April 1990.

[24] I. Pitas and A.N. Venetsanopoulos, *Nonlinear Filters in Image Processing: Principles and Applications*, Kluwer Academic Publishers, Boston, 1990.

[25] G. Sapiro and D. Malah, "Morphological Image Coding Based on a Geometric Sampling Theorem and a Modified Skeleton Representation", *Journal of Visual Communication and Image Representation*, Vol. 5, No. 1, pp. 29-40, March 1994.

[26] D. Schonfeld and J. Goutsias, "Morphological Representation of Discrete and Binary Images", *Trans. Signal Processing*, Vol. 39, No. 6, pp. 1369-1379, June 1991.

[27] J. Serra, *Image Analysis and Mathematical Morphology.* London: Academic Press, 1982.

[28] J. Serra, *Image Analysis and Mathematical Morphology, Vol.2: Theoretical Advances.* New York: Academic Press, 1988.

[29] J. Serra, "Skeleton Decompositions", *SPIE Vol. 1769, Image Algebra and Morphological Image Processing III*, pp. 376-386, July 1992.

[30] J. Serra, "Connected Operators and Pyramids", *SPIE Vol. 2030, Image Algebra and Mathematical Morphology*, San Diego, pp. 65-76, 1993.

[31] D. Shaked, *Symmetry Invariance and Evolution in Planar Shape Analysis*, D.Sc. Thesis (in English), Department of Electrical Engineering, Technion, Israel, June 1995.

[32] S.R. Sternberg, "Grayscale Morphology", *CVGIP*, Vol. 35, No. 3, pp.333-355, Sept. 1986.

[33] Ph. Salembier, F. Marqués, and A. Gasull, "Coding of Partition Sequences", chapter 4 in *Video Coding: The Second Generation Approach*, L. Torres and M. Kunt (Eds.), Boston: Kluwer Academic, 1996.

Coder	Bits/pixel
Runlength + Huffman	0.152
Quadtree	0.131
Chain-Code	0.091
Skeleton (proposed)	**0.071**

Table 1: Lossless compression rates, in bpp, of the proposed skeleton coder and other known schemes, for the image "Tools".

CCITT Images	G3D1 (MH)	d_8 Skeleton	G3D2 (MR, $K = 4$)	**Proposed Skeleton**	G4 (MMR)	Non-Progressive JBIG
#1	37423	28261	25967	**20405**	18103	14715
#2	34367	19058	19656	**12681**	10803	8545
#3	65034	49018	40797	**37535**	28706	21988
#4	108075	102848	81815	**82194**	69275	54356
#5	68317	52476	44157	**40259**	32222	25877
#6	51171	30658	28245	**24615**	16651	12589
#7	106420	112301	81465	**83398**	69282	56253
#8	62806	35965	33025	**24815**	19114	14278

Table 2: File sizes of compressed facsimile standard CCITT documents, obtained by the proposed skeleton algorithm, compared to previous skeleton-Based coder and existing standards.

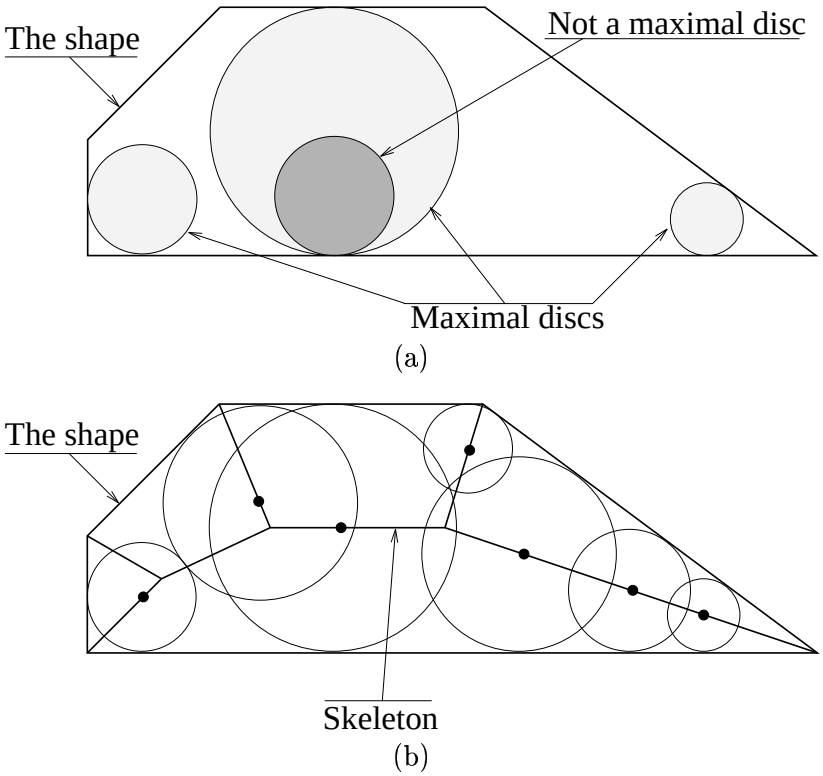

Figure 1: The definition of skeleton in terms of *maximal discs*. (a) Maximal discs in a shape, (b) the skeleton as the centers of all the maximal discs.

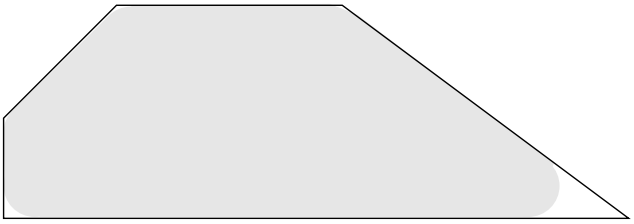

Figure 2: Partial reconstruction of the skeleton representation. Simplification of the shape is obtained by removing skeleton points related to maximal discs with value smaller than a threshold.

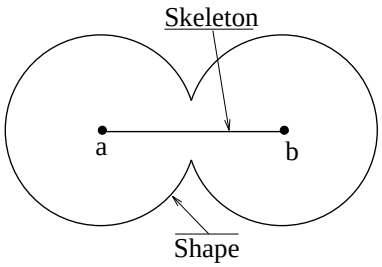

Figure 3: Skeleton Redundancy. Only the points a and b are not redundant in this skeleton representation.

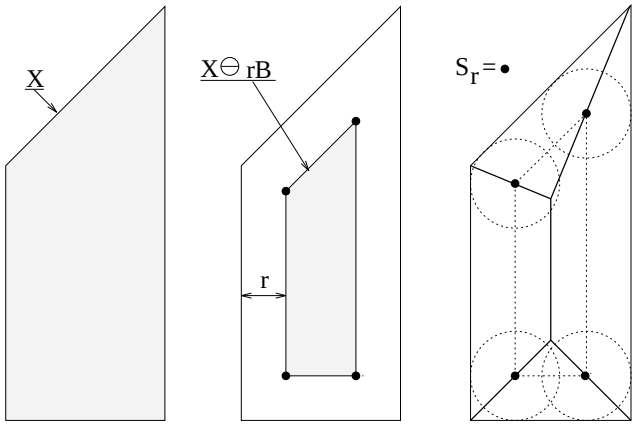

Figure 4: Skeleton calculation by morphological operations. The skeleton points are the "vertices" of the regions $X \ominus rB$, for $r > 0$.

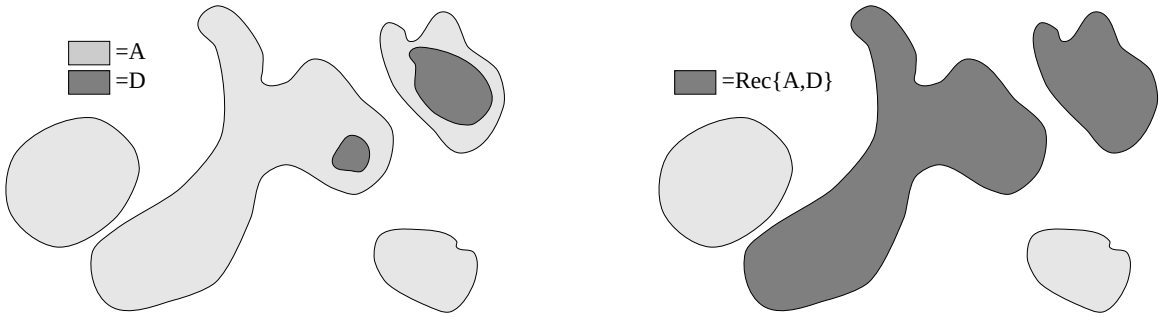

Figure 5: The reconstruction operator. (a) Two sets A and D, such that $D \subset A$. (b) The result of reconstruction of A from D, under an infinitesimal circular structuring element B.

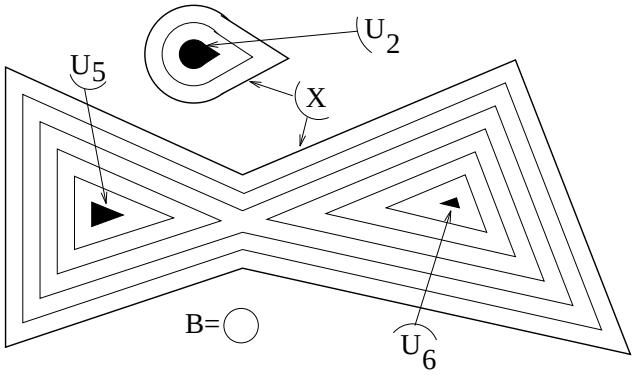

Figure 6: Discrete ultimate erosions U_n of a set X composed of two connected components. The succession of internal lines represents the erosions of X by nB, $n > 0$.

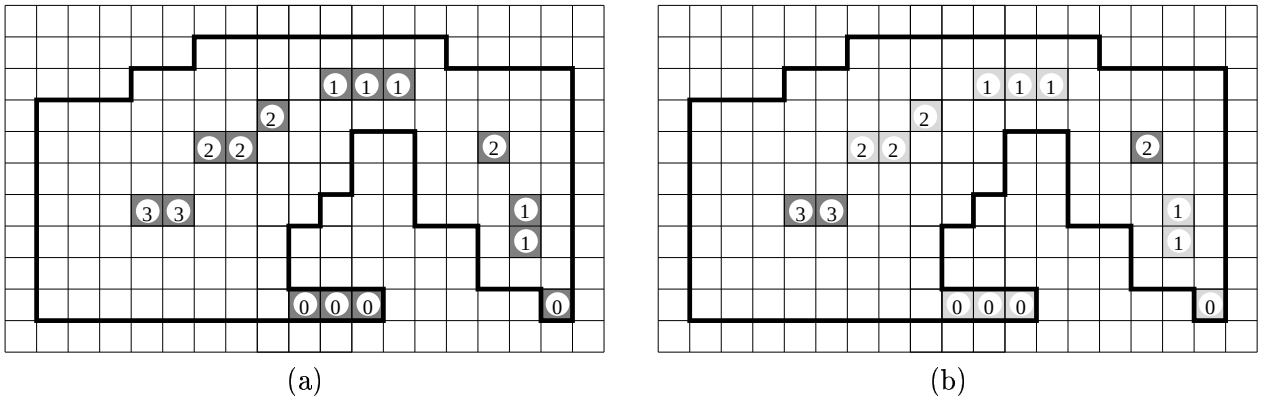

Figure 7: (a) A binary image (indicated by the thick line), and its skeleton points. The numbers indicate the corresponding radii. (b) the ultimate erosions (the darker points).

Figure 8: Skeleton and ultimate erosions of a portion of the image "Coffee Grains". The ultimate erosions are the black skeleton points.

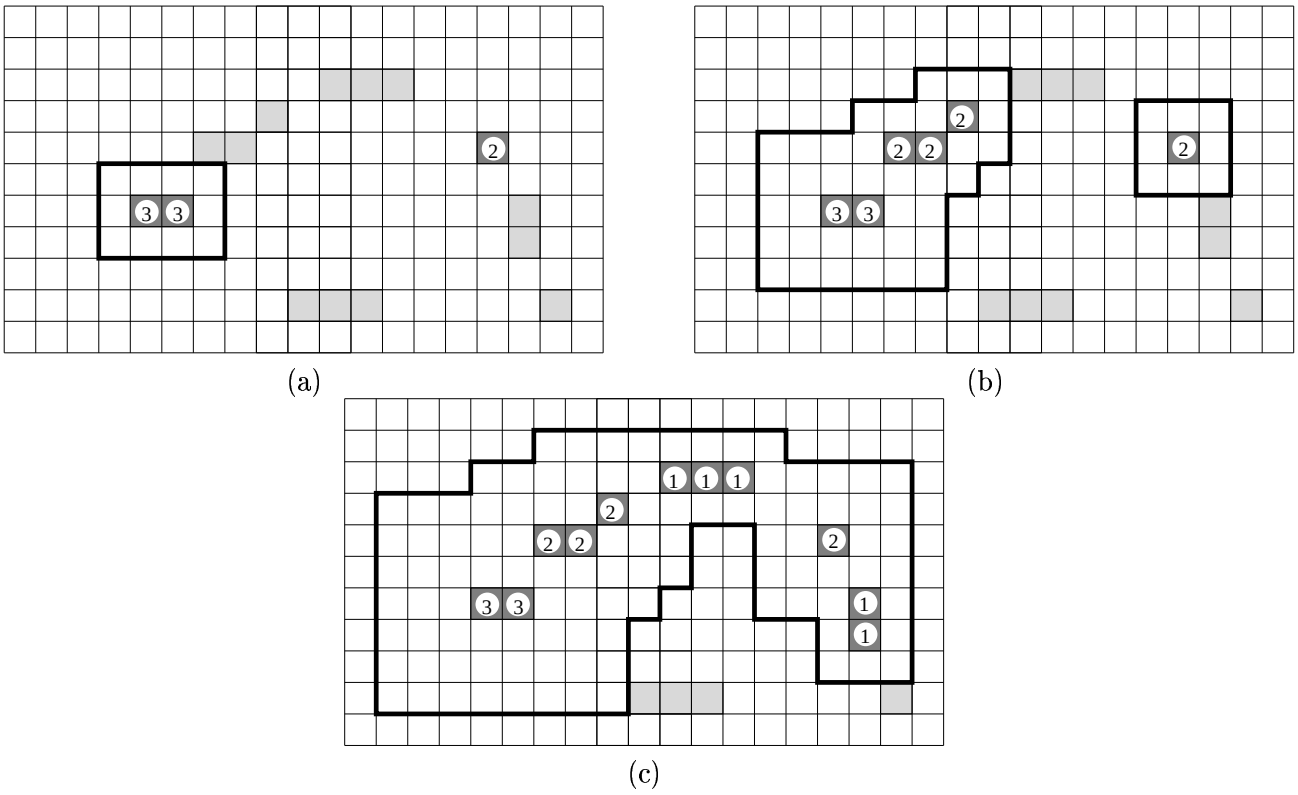

Figure 9: Reconstruction algorithm from a skeleton with sampled quench function. The skeleton is the same as in Fig. 7. $N = 3$, and the ultimate erosion points are indicated by the dark gray pixels in (a). (a) Step n=2 of the algorithm, (b) step n=1 of the algorithm, (c) step n=0 of the algorithm. In (a), (b), and (c), Z is indicated by the thick line, and the points in S_n are those connected components of S (the light gray pixels) that touch Z, plus U_n (in this case, U_0 and U_1 are empty).

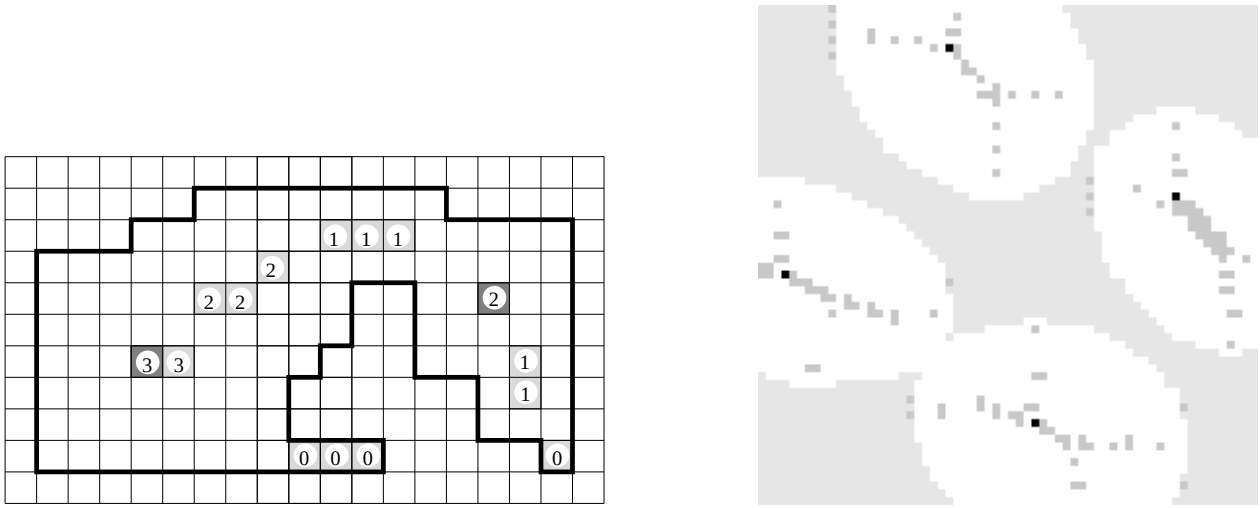

Figure 10: In the above examples, the dark points are the only ones in the respective skeletons that need to have their radius coded, according to Corollary 2. In the right image, there are only 4 of these points.

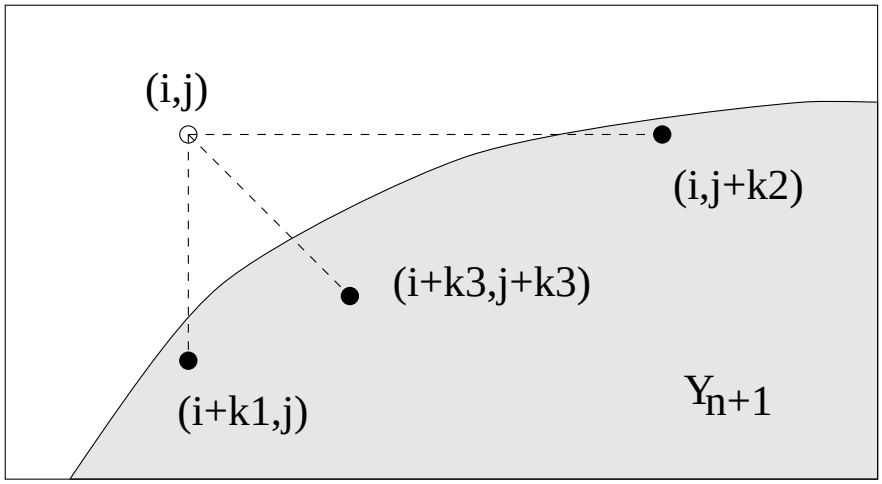

Figure 11: A point (i, j) predicted not to belong to S_n according to Corollary 5.

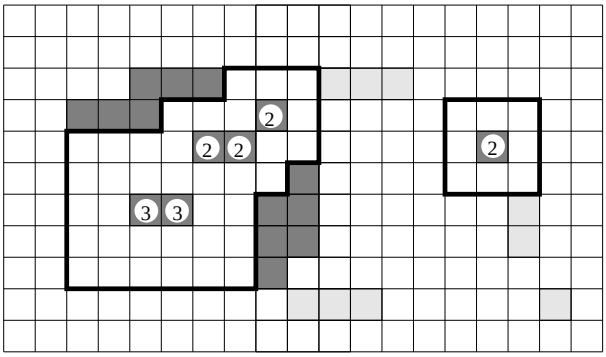

Figure 12: An example of deterministic prediction. Here, $n = 1$, and the thick line indicates Y_{n+1}. The dark points cannot be skeleton points in S_1, according to Corollary 5.

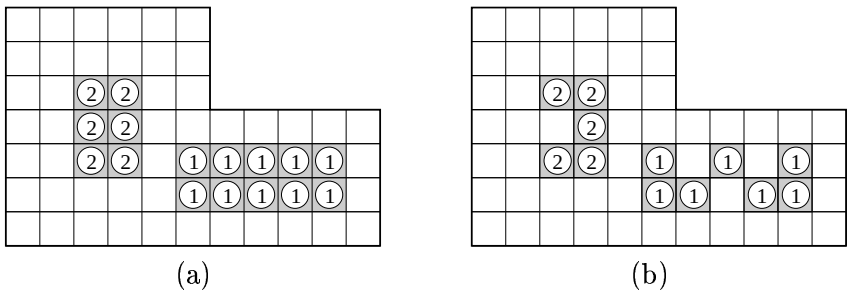

Figure 13: A Redundancy Reduction scheme for a skeleton calculated with a 3×3-squared structuring element. (a) Original skeleton, (b) Reduced skeleton.

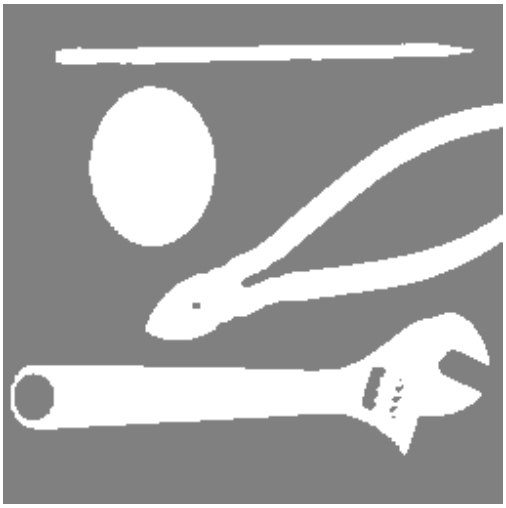

Figure 14: Binary image "Tools" (256×256 pixels), used for the compression simulations.